Advances in Engineering Software 115 (2018) 112–125

Contents lists available at ScienceDirect

Advances in Engineering Software

journal homepage: www.elsevier.com/locate/advengsoft

Research paper

Predicting compressive strength of lightweight foamed concrete using extreme learning machine model

Zaher Mundher Yaseen[a,b,*], Ravinesh C. Deo[c], Ameer Hilal[d], Abbas M. Abd[e], Laura Cornejo Bueno[f], Sancho Salcedo-Sanz[f], Moncef L. Nehdi[g]

[a] Civil and Structural Engineering Department, Faculty of Engineering and Built Environment, Universiti Kebangsaan Malaysia, 43600 UKM Bangi, Selangor Darul Ehsan, Malaysia
[b] Dams and Water Resources Department, College Of Engineering, University of Anbar, Ramadi, Iraq
[c] School of Agricultural, Computational and Environmental Sciences, Institute of Agriculture and Environment (IAg&E), University of Southern Queensland, QLD 4300, Australia
[d] Civil Engineering Department, College of Engineering, University of Anbar, Iraq
[e] Architectural Engineering Department, College of Engineering, University of Diyala, Iraq
[f] Department of Signal Processing and Communications, Universidad de Alcalá, Madrid, Spain
[g] Department of Civil and Environmental Engineering, Western University, London, Canada

ARTICLE INFO

Keywords:
Foamed concrete
Compressive strength
Prediction
ELM
MARS
M5 Tree
SVR

ABSTRACT

In this research, a machine learning model namely extreme learning machine (ELM) is proposed to predict the compressive strength of foamed concrete. The potential of the ELM model is validated in comparison with multivariate adaptive regression spline (MARS), M5 Tree models and support vector regression (SVR). The Lightweight foamed concrete is produced via creating a cellular structure in a cementitious matrix during the mixing process, and is widely used in heat insulation, sound attenuation, roofing, tunneling and geotechnical applications. Achieving product consistency and accurate predictability of its performance is key to the success of this technology. In the present study, an experimental database encompassing pertinent data retrieved from several previous studies has been created and utilized to train and validate the ELM, MARS, M5 Tree and SVR machine learning models. The input parameters for the predictive models include the cement content, oven dry density, water-to-binder ratio and foamed volume. The predictive accuracy of the four models has been assessed via several statistical score indicators. The results showed that the proposed ELM model achieved an adequate level of prediction accuracy, improving MARS, M5 Tree and SVR models. Hence, the ELM model could be employed as a reliable and accurate data intelligent approach for predicting the compressive strength of foamed concrete, saving laborious trial batches required to attain the desired product quality.

1. Background

Foamed concrete is a versatile material consisting of either Portland cement paste or mortar, with a homogeneous cellular structure created via inducing air voids during the mixing process [1]. Being lightweight with desirable sound attenuation and heat insulation characteristics, the foamed concrete can be made more sustainable and eco-efficient through partial or full replacement of fine aggregates with recycled by-products [2]. To ensure its optimal benefits, there have been attempts to enhance the mechanical properties of foamed concrete, particularly for structural purposes beyond the traditional filling and insulation applications.

The compressive strength of foamed concrete dramatically decreases with a reduction in its density. The water-to-cement and sand-to-cement ratios, curing regime, distribution of voids and type of foaming agent used are the key parameters affecting the mechanical strength of foamed concrete [3]. Kearsley and Wainwright [4] reported that the compressive strength of foamed concrete is primary a function of its dry density, while the percentage of fly ash partial replacement for cement had little effect on compressive strength. Hilal et al. [5] investigated the effect of different additives on the compressive strength of foamed concrete, the influence of the air-void size and shape parameters, and changes its actual microstructure. This study concluded that the enhancement of the void structure can contribute to the strength of the foamed concrete.

Several other studies have investigated properties of foamed

* Corresponding author.
E-mail addresses: zahermundher@gmail.com, p77769@siswa.ukm.edu.my (Z.M. Yaseen).

http://dx.doi.org/10.1016/j.advengsoft.2017.09.004
Received 20 April 2017; Received in revised form 23 July 2017; Accepted 14 September 2017
Available online 21 September 2017
0965-9978/

concrete, with or without additives and admixtures including mechanical strength [4,6–9], durability [10–13], pore structure [14–16], fracture properties [17,18] and its structural properties in a composite system [2,19]. Such studies have investigated the ability to predict the compressive strength of foamed concrete from its mixture constituents, with a general view to attain a superior quality of the product. For instance, Narayanan and Ramamurthy [20] and Nehdi et al. [21] have suggested that the influence of mixture constituents (by its volume) of cellular concrete on its compressive strength can be represented by Feret's formula. This in fact, relates the compressive strength (f_{cc}) to water-to-cement ratio (w/c) and air-to-cement ratio (a/c) as follows:

$$f_{cc} = k\left(\frac{1}{1+\frac{w}{c}+\frac{a}{c}}\right)^{m} \quad (1)$$

where k and m are empirical constants.

Narayanan and Ramamurthy [20] reported three proposed strength prediction models based on the porosity of aerated concrete. In a study to investigate the effect of the water-to-cementitious materials ratio on the void system and mechanical properties of foamed concrete, [78] proposed the following relationship between the compressive strength (f_{cc}) of foamed concrete and the air content (A) as a function of the compressive strength of the cement paste (f_c):

$$f_{cc} = 1.048\, f_c\, (1-A)^{2.793} \quad (2)$$

The following equation expresses the relationship between compressive strength (fc) of cement paste and effective water-to-cement ratio (w/c) as well as curing time (t):

$$f_c = 88.04 + 6.569\ln(t) - 130.5\ w/c \quad (3)$$

Moreover, the effect of the binder ratio on the compressive strength of foamed concrete was derived by Kearsley and Wainwright [4] as follows:

$$f_{cc} = 1.172\, f_c\, \propto_b^{3.7} \quad (4)$$

where: f_{cc} is the compressive strength of foamed concrete, f_c is the compressive strength of the cement paste calculated from Eq. (3) and α_b is the binder ratio (by volume).

In view of the above formulations, the prediction of compressive strength relies on a number of parameters, whose contribution to the overall material needs to be optimized. Due to the large differences between the calculated and actual compressive strength results, Kearsley and Wainwright [4] concluded that there may be other factors than age, effective water-to-cement ratio and binder ratio that have significant effect on the compressive strength of foamed concrete. They observed that such differences between calculated and actual strengths increased with decreasing density (i.e. with increasing foam volume), indicating that the void system (total volume and size distribution of voids) are influential on the compressive strength of foamed concrete. Assuming that the cement paste in the foamed concrete has the same strength of that of the un-foamed mortar and noting that the effect of the age and w/c are already taken into account in Eq. (3), the effect of the foam volume can be taken into account by adopting the density ratio, which is the ratio between the dry density of the foamed concrete and that of the un-foamed mixture before adding the foam.

The relationship between compressive strength of foamed concrete (f_{cc}) and the dry density ratio (α_d) was derived via regression analysis by Kearsley and Wainwright [22] as follows:

$$f_{cc} = f_c(-0.324 + 1.325\ \propto_d)^2 \quad (5)$$

Earlier research by Nehdi et al. [21] implemented novel soft computing approaches (i.e. artificial neural networks (ANN)) in predicting the compressive strength of pre-formed foam cellular concrete. They applied four key input variables, including the cement content, water-to-cementitious materials ratio, sand-to-cementitious materials ratio and foam-to-cementitious materials ratio. It was found that the ANN model provided a powerful tool for predicting the compressive strength of foamed concrete. In a somewhat related study, Khan [23] also reported the applicability of ANN for the prediction of the compressive strength, tensile strength, gas permeability and chloride ion penetration of high performance concrete. A comparative investigation between ANN model and linear regression model for estimating the compressive strength of steel fiber-added lightweight concrete was carried out by [24]. In this work, it was found that the ANN model outperformed the linear regression model yielding more accurate estimation. Altun, Kişi [25] estimated the compressive strength of concrete incorporating various amounts of blast furnace slag and fly ash, based on the properties of the additives and values obtained by non-destructive testing rebound number and ultrasonic pulse velocity. The application of ANN to predicting compressive strength has thus shown great potential, particularly for calculating nonlinear functional relationships, for which classical methods cannot be applied. Many other researchers have explored the applicability of ANN models in predicting the concrete strength [26–29]. All reported studies emphasized the reliability of ANN in predicting compressive concrete strength. Yet, such models remain ``black box" tools, requiring internal parameters, along with time consuming training and validation.

Over the past five years, the implementations of the non-tuned machine learning model ``i.e., ELM" have shown a noticeable progress in multidisciplinary of science and engineering fields. This is due to its advantages (particularly over conventional artificial neural network algorithms) such as the randomly initiated hidden neurons without the need for iterative tuning process for free parameters or connections between hidden and output layer. Consequently, ELM is remarkably efficient to reach a global optimum, following universal approximation capability of single layer feed-forward network [30,31]. Also, this model is featured by the efficiency and generalization performance over traditional learning algorithms (*e.g.*, SVMs or ANNs) as revealed in the estimation problems in many different fields (e.g., [32–35]). For more details on advanced theoretical perspectives, including the interpolation theory, universal approximation capability and generalization ability of ELMs, the readers can refer to many other excellent reviews (*e.g.*, [30,36,37]).

In the present research paper, the implementation of the machine learning regression model, namely extreme learning machine (ELM) is developed for the first time to predict the compressive strength of foamed concrete. The efficiency of the ELM model is verified against couple of highly robust regression models including multivariate adaptive regression splines (MARS), M5 Tree and support vector regression (SVR). The modeling is conducted using an experimental database retrieved from previous published studies available in the open literature.

The rest of the article is structured in the following way: In the next section, the machine learning models considered in this paper are described. In Section 3, the description of the experimental dataset is presented. The model's development and prediction skills metrics are indicated in Sections 4 and 5. The application and results are discussed in Section 6. Finally, the conclusion and remarks are presented in the last section of conclusions.

2. Methodological background

2.1. Extreme learning machine

The Extreme Learning Machine (ELM), is a neural network-based model, and an innovative new data-driven tool that utilizes a state-of-the-art single-layer feed forward network (SLFN) algorithm to yield a closed-form solution to the output weights through a least squares solution (after fixing the hidden layer weights and biases). It is drawn from a continuous probability distribution function [31] rather than using an iterative solution adopted by a conventional feed-forward ANN model. The major advantage of the ELM model is the lesser complexity

involved in its design and in its ability to solve regression (or classification) problems in less time [38] since the weights and biases within its hidden neurons are randomized, and the output has a unique least-square solution solved by Moore-Penrose inverse function [36]. This avoids the need for iterative training methods (e.g. ANN models) that tend to collapse to local, rather than global, minima in the predictor dataset.

In modelling the data using an ELM model, a simple three-step building procedure is employed as follows: (i) construct hidden layer weights and biases randomly (rather than iteratively as in the case of an ANN model; (ii) progress the inputs through the hidden layer parameters to produce the hidden layer output matrix; and (iii) estimate the output weights by inverting the hidden layer output matrix where the Moore-Penrose generalized inverse matrix is used and then compute its product with the response variable (i.e., solving a set of linear equations). This process requires the randomization of hidden neurons once the hidden neuron nodes have been identified. Normally, the hidden neurons are identified by trial-and-error over a cross-validation dataset. With a greater foresight for real-time implementation, an ELM offers a distinct advantage over other models that suffer from slow convergence rates, inferior generalization, local minima issues, over-fitting of data and iterative tuning. The fast and improved performance of an ELM is thus advantageous in real-time applications [34,39].

Fig. 1 illustrates an ELM model. In this paper, the ELM model is adopted to train the predictor/target data pairs (with cement, oven dry density, water-to-binder ratio and foam volume) as the predictors $\boldsymbol{x}_i$ and compressive strength as the target y_i. For a set of d-dimensional vectors defined for i $i = 1, 2, \ldots, N$ training samples, the SLFN with L hidden neurons is mathematically expressed as follows [36]:

$$f_L(\mathbf{x}) = \sum_{i=1}^{L} h_i(\mathbf{x})\beta_i = h(\mathbf{x})\beta \tag{6}$$

Note that $\beta = [\beta_1, \beta_2 \ldots \beta_L]^T$ is the output weight matrix between the hidden neurons and output neurons; $h(\mathbf{x}) = [h_1, h_2 \ldots h_L]$ is the hidden neuron outputs that represent the randomized hidden features of predictor x_i; $h_i(\boldsymbol{x})$ is the i^{th} hidden neuron. The output functions of the hidden neurons, $h_i(\mathbf{x})$ can be represented as follows [38]:

$$h_i(\mathbf{x}) = G(\mathbf{a}_i, b_i, \mathbf{x}), \quad \mathbf{a}_i \in R^d, b_i \in R \tag{7}$$

$G(\boldsymbol{a}_i, b_i, \mathbf{x})$, which is defined using hidden neuron parameters $(\boldsymbol{a}, b)$, is a non-linear piecewise continuous function that must satisfy the ELM approximation theorem [31,36,38]. The sigmoid equation, which has been adopted widely in neural network-based modelling, was used herein for developing the ELM model as expressed below [33]:

$$\text{Log Sigmoid} \Rightarrow G(\mathbf{a}, b, \mathbf{x}) = \frac{1}{1 + \exp(-\mathbf{a}x + b)} \tag{8}$$

Huang et al. [38] state that the approximation error must be minimized when solving for the weights connecting the hidden and output layer $(\boldsymbol{\beta})$ using least square fitting [38]:

$$\min_{\beta \in R^{L \times m}} \|\mathbf{H}\beta - \mathbf{T}\|^2 \tag{9}$$

In Eq. (9), the term $||Hb\text{-}T||$ is the Frobenius norm and $\mathbf{H}$ is the randomized hidden layer output matrix of the form [38]:

$$\mathbf{H} = \begin{bmatrix} g(x_1) \\ \vdots \\ g(x_N) \end{bmatrix} = \begin{bmatrix} g_1(a_1x_1 + b_1) & \cdots & g_L(a_Lx_1 + b_L) \\ \vdots & \cdots & \vdots \\ g_1(a_Nx_N + b_1) & & g_L(a_Lx_N + b_L) \end{bmatrix} \tag{10}$$

and the target matrix in the data training period is expressed as [38]:

$$\mathbf{T} = \begin{bmatrix} \mathbf{t}_1^T \\ \vdots \\ \mathbf{t}_N^T \end{bmatrix} = \begin{bmatrix} t_{11} & \cdots & t_{1m} \\ \vdots & & \\ t_{N1} & \cdots & t_{Nm} \end{bmatrix} \tag{11}$$

An optimal solution is given by solving a system of linear equations [40]:

$$\beta^* = \mathbf{H}^+\mathbf{T} \tag{12}$$

where $\boldsymbol{H}^+$ is the Moore-Penrose generalized inverse function (+) [36]. The optimal solution is then used in (12) to issue a prediction for any given input vector, $\boldsymbol{x}$.

2.2. Multivariate adaptive regression splines

To evaluate an ELM model with alternative data-driven techniques for prediction of compressive strength, a multivariate adaptive

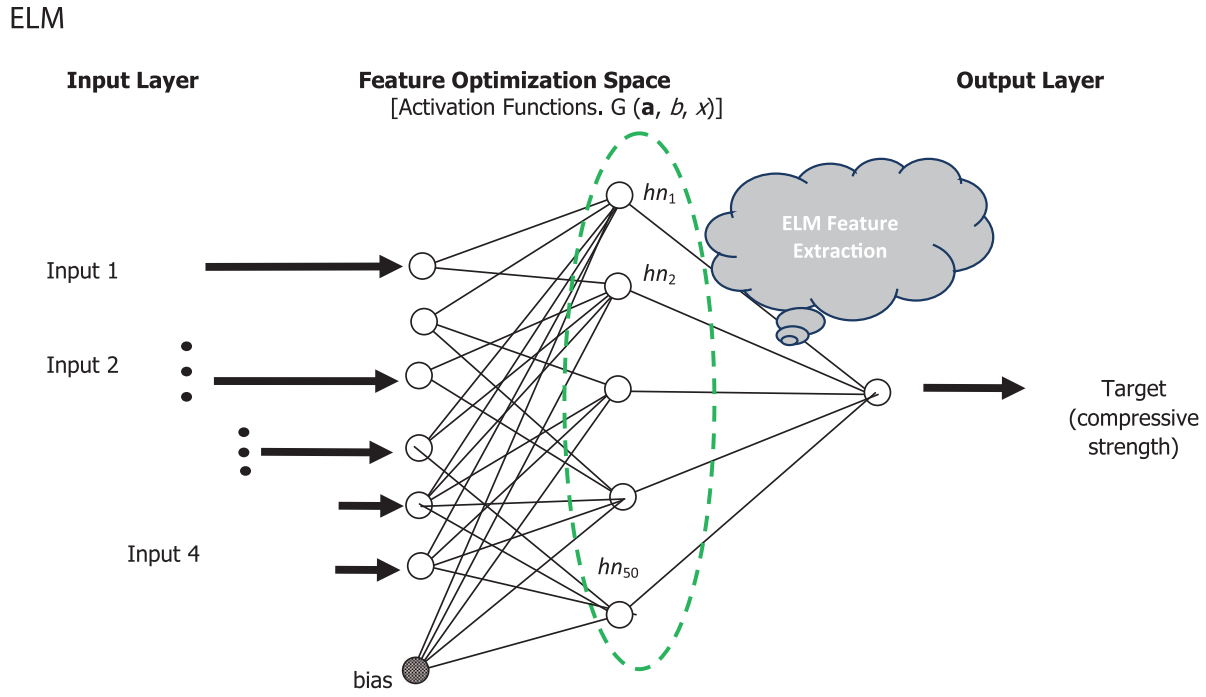

Fig. 1. Extreme Learning Machine algorithm structure.

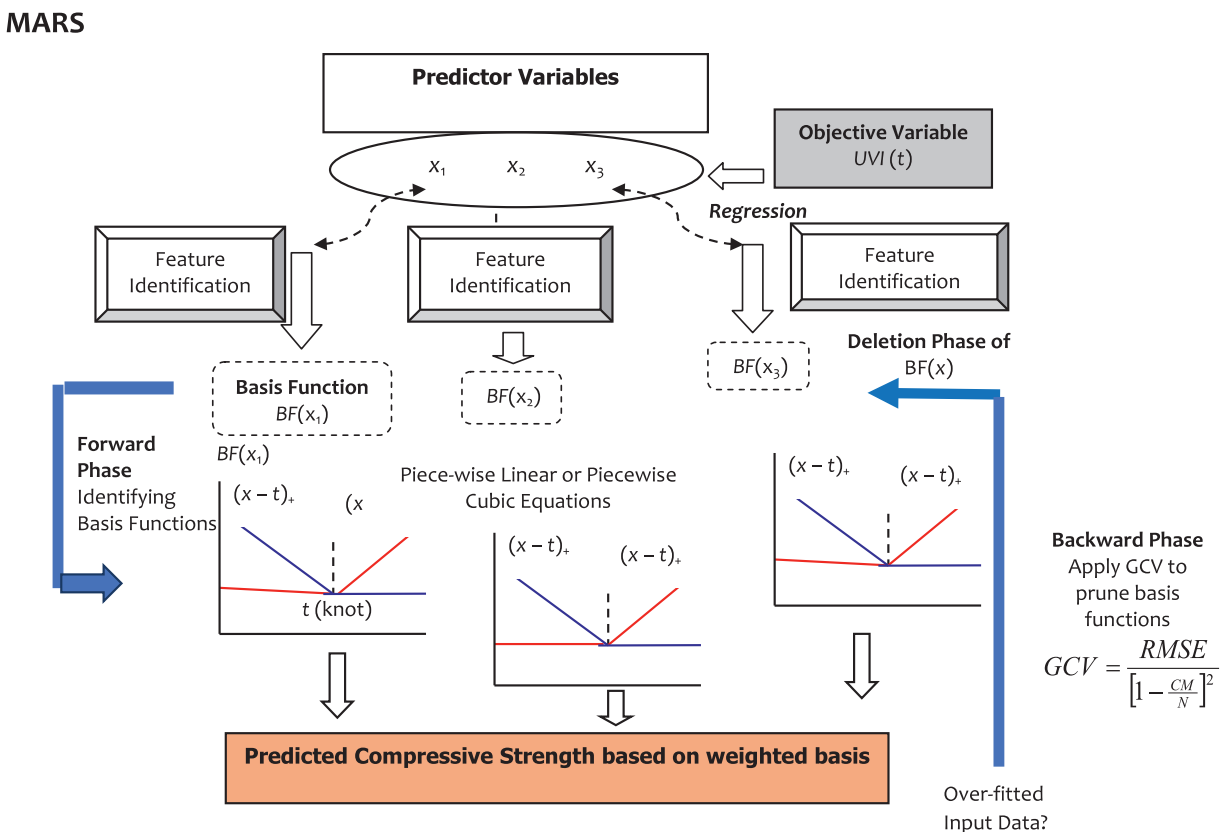

Fig. 2. Multivariate adaptive regression splines model architecture.

regression spline (MARS) model [41], that operates differently from neural networks, has been adopted. Fig. 2 shows a schematic view of MARS, which is used in non-linear estimation problems [42–51]. There has been so far no application accessible in the open literature of this model for estimating concrete compressive strength, which has also motivated the present study.

As MARS considers multivariate data, it can analyze the contribution of basis functions from predictors, where interactive effects from explanatory terms are utilized for simulating the predictand [52]. MARS determines the importance of predictors that affect the predictand, and thus, allows a modeler to explore non-linear relationships embedded in predictors and predictand [43]. It performs a selection of the best regressors and implements an automatic smoothing of predictor data [48]. MARS does not require assumptions on a statistical relationship [41,53], but instead it generates forecasts based on learned relationships constructed using several splines [41]. For each spline, inputs are split into subgroups and knots, and are located between $\boldsymbol{x}$ and the interval in the same $\boldsymbol{x}$ to separate the subgroup [41,54].

Between any two knots, MARS characterizes the data globally or via piecewise (cubic or linear) functions so that the basis functions in the adjacent domain intersect at the knot. This provides MARS flexibility to consider bends, thresholds and departures from linearity found in the predictor-predictand matrix [55]. In contrast to conventional models, MARS creates a bended regression line to fit $\boldsymbol{x}$ data from subgroup to subgroup and spline to spline [42], but this limit is deduced by trial-and-error. The basis functions, $BF(x)$ are determined from the *SZA* and are projected on the predictand (UVI) vector [42,48]. Suppose $\boldsymbol{X}$ is the vector $(\boldsymbol{x_1}, \boldsymbol{x_2}\ldots \boldsymbol{x_N})$, then:

$$\mathbf{Y} = f(\mathbf{X}) + \xi \tag{13}$$

where ξ is the distribution of error [43,44] and N is the number of training datum points.

MARS approximates $f(.)$ by applying $BF(x)$ with a piecewise function: max (0, $\boldsymbol{x}$–c) where a knot is found to occur at the position c [55]. The max (.) means that only the positive part of (.) is used, otherwise it is zero, concordant with:

$$\max(0, x-c) = \begin{cases} x-c, & if\ c \geq t \\ 0, & otherwise \end{cases} \tag{14}$$

$f(\mathbf{X})$ is constructed as a linear combination of $BF(x)$ and its interactions:

$$f(\mathbf{X}) = \beta_o + \sum_{n=1}^{N} \beta_n BF(\mathbf{X}) \tag{15}$$

where β is a constant estimated using the least-square method and $f(\mathbf{X})$ is applied as a forward-backward stepwise method to identify the knots where the function varies [48]. At the end of forward phase, a large model is generated, which in fact may over-fit the trained data. A backward phase is engaged by deleting at least one basis function as per the Generalized Cross Validation (GCV) until the model has only the intercept term. GCV, which is a regularization metric and is given by [56]:

$$GCV = \frac{RMSE}{\left[1-\frac{CM}{N}\right]^2} \tag{16}$$

Here, the *RMSE* is the root mean squared error in the trained data, *CM* is the penalty and d is the cost penalty factor of each basis function optimization:

$$CM = M + dM \tag{17}$$

It is noteworthy that Eq. (14) estimates how well MARS fits new (forecasted) data [43]. To optimize the basis functions based on the lowest GCV, some basis functions are finally deleted [44, 57].

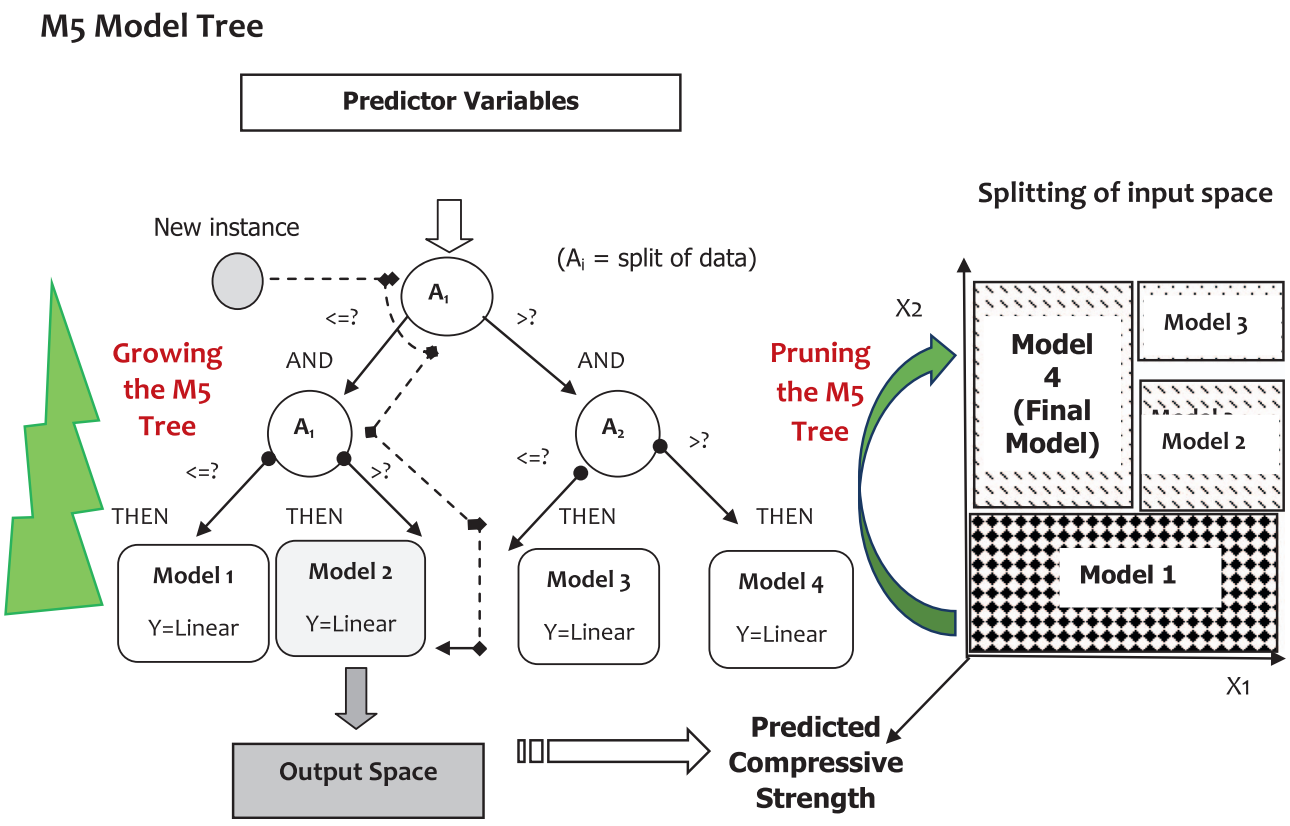

Fig. 3. M5 Tree predictive model based structure.

2.3. M5 model tree

In the present study, the M5 Model tree has also been deployed as a data-driven model to compare the ELM and MARS [58]. This is a hierarchical model based on a binary decision framework that employs linear regression at terminal (leaf) nodes to investigate relationships in the predictor-predictand matrix [46,59]. To develop an M5 Model tree, two processes are applied [60]. First, the input data are split in subsets to create a decision tree for patterns/attributes in the input-output dataset. Subsequently, a model tree is constructed. Fig. 3 exhibits a schematic view of an M5 Model Tree.

Consider an *N*-sample, d-dimensional training matrix characterized by (input) attributes associated with the predictand. An M5 Tree model aims at relating a target value of the training cases to the predictor [61]. Using divide-and-conquer rule, a tree-model is constructed where *N* points are associated with a leaf or a test criterion that splits them into subsets corresponding to a test outcome. This process is applied recursively where subsets are created following a criterion depending on the standard deviation of class values and the reduction in error, σ_R [44,61]:

$$\sigma_R = \sigma(\Lambda) - \sum \left(\frac{\Lambda_i}{\Lambda}\sigma(\Lambda_i)\right) \tag{18}$$

Λ is a set of examples which reach the node; Λ_i is the subset of examples that have the i^{th} outcome of the potential set.

When maximum splits for data attributes are attained, a regression tree is used to select them to optimize the M5 Tree model with the minimum value of σ_R. The splitting ceases when the class value of all instances reaching a node do not vary or that just a few instances remain. It so turns out that the perpetual division rule applied to input data can lead to a very large, overelaborate network of structures that must be pruned back. If a model is constructed from several points, smoothing is applied to compensate for any abrupt discontinuities that occur between adjacent models at the leaves of the pruned tree [44,61]. This improves the accuracy of the fine-tuned model. During smoothing, linear equations are updated so that the forecasted output in relation to its corresponding input vector becomes closer, as outlined in greater details elsewhere (e.g. Quinlan, [58] and Witten and Frank, [62].

2.4. Support vector regression

As another very popular regression model applied to evaluate the preciseness of ELM, the support vector regression (SVR), which operates on a statistical modelling framework, is applied [63,64]. In contrast to neural network based, multivariate regressions and tree-based approaches presented earlier, the SVR model is based on structural risk minimization principle [65] that forces a regularization constraint on the model's weight for feature extraction. In our study, we used the least square SVR that alleviates convex quadratic programming associated with conventional support vector machines (SVM) [66,67].

SVR solves the regression problem as a set of linear equations, as an advantage, providing faster training process, and better higher stability and modelling accuracy (Sadri and Burn, 2012). The SVR model is able to yield global solution by minimizing the error function, and therefore, presents some advantage over the gradient based models (e.g. an artificial neural network) [68,69]. A kernel function (*K*) and its parameters are optimised so that a bound on Vapnik–Chervonenkis dimension is minimized to yield stable solutions through the use of least square regressions [70].

Mathematically, SVR model is stated as follows. If predictors $X = \boldsymbol{x}_i$ and compressive strength as the target $Y = y_i$., then SVR model is written as:[32, 46, 71]

$$\mathbf{Y}(\mathbf{X}) = f(\mathbf{B}) = w^T \Psi(\mathbf{X}) + \mathrm{B} \tag{19}$$

where w, ψ and B = weight vectors, mapping functions applied for feature extraction and bias terms, respectively [66,72].

In accordance with the function's estimation error, the SVR model applies structural risk minimisation to the *J* term, which is as follows:

$$\min J(w, e) = \frac{1}{2}w^T w + \frac{C}{2}\sum_{i=1}^{m} e_i^2 \tag{20}$$

where $e_i^2$is the quadratic loss, W is the weight and C is the regularization parameter. In principle, Eq. (20) follows the following [44]:

$$y_i = w^T\Psi(x_i) + \mathrm{B} + e_i\,(i = 1,\ 2,\ \ldots,\ m) \tag{21}$$

During the modelling, we need to solve for the model parameters such that a Lagrangian multiplier ($\alpha_i \in R^N$) needs to be applied [44]:

$$\Gamma(w,\ \mathrm{B},\ e,\ C) = J(w,\ e) - \sum_{i=1}^{m}\alpha_i\{w^T\Psi(x_i) + b + e_i - y_i\} \tag{22}$$

In the next step, the conditions for solving the parameters are implemented by taking the partial-derivatives of the loss function (i.e. $\Gamma(W, B, e, \alpha)$) with respect to each term (i.e. W, B, e, α) [44]:

$$\begin{cases} w = \sum_{i=1}^{m}\alpha_i\Psi(x_i) \\ \sum_{i=1}^{m}\alpha_i = 0 \\ \alpha_i = Ce_i \\ w^T\Psi(x_i) + \mathrm{B} + e_i - y_i = 0 \end{cases} \tag{23}$$

where $\psi(x)$ is a nonlinear mapping function related to kernel function, expressed as [66]:

$$\begin{bmatrix} 0 & -Y^T \\ Y & \Omega\Omega^T + \frac{I}{C} \end{bmatrix}\begin{bmatrix} \mathrm{B} \\ \alpha \end{bmatrix} = \begin{bmatrix} 0 \\ I \end{bmatrix} \tag{24}$$

In Eq. (24), $Y = \{y_1,\ldots, y_m\}$, $\Omega = \Psi(x_1)^T y_1,\ldots, \Psi(x_m)^T y_m$, $I = \{1, \ldots, 1\}$, $\alpha = \{\alpha_1,\ldots, \alpha_l\}$and Ω is applied as the kernel function satisfying Mercer's theorem [73]. SVR model is therefore expressed as:

$$f(x) = \sum_{i=1}^{m}\alpha_i\Omega(x, x_i) + \mathrm{B} \tag{25}$$

and the radial basis kernel function (RBF) is expressed as:

$$\Omega(x, x_i) = \exp\left(\frac{-\|x - x_i\|^2}{2\sigma^2}\right) \tag{26}$$

In Eq. (26), σ is the kernel width and both C and σ are determined by a suitable grid search (i.e. hyperparameters) which is similar to the determination of hidden neurons in a neural network model [74–77].

3. Experimental data set description

In this paper, conventional foamed concrete data consists of either cement paste (mixture of cement and water) or mortar (mixture of cement, water, and sand) with a homogenous pore structure created by adding a certain volume of foam bubbles. To enhance specific properties of foamed concrete, including compressive strength, additives such as silica fume and fly ash can be deployed. Moreover, water reducers and superplasticizers can be incorporated to lower the water-to-binder ratio, thus enhancing compressive strength. It was also found that adding glass, steel, carbon and synthetic fibers can help enhance the tensile strength, flexural performance and toughness of foamed concrete, while the effect on compressive strength is less tangible [2]. Hence, the addition of fibers, was not considered as an influential parameter on compressive strength in the present study. Conversely, the effect of superplasticizers was implicitly accounted for via the water content used in the mixing process. Supplementary cementitious materials such fly ash and silica fume were included in the cementitious content and their effect on compressive strength was considered.

The database used herein in model development was retrieved from various studies in the open literature on foamed concrete having density in the range of (600–1800 kg/m^3) with different volumes of added foam, various density and mixture constituents [4,78,79]. Appendix 1 shows the dataset used in the construction of the ELM and the counterpart (comparative) models. In total, 91 data points were used to build and validate the data intelligent models, divided into two different sets: training and validation/testing. Input data included cementitious material content, oven dry density, water/binder ratio and foam volume, while the output data represents the predicted compressive strength (S).

4. Models development and construction

To predict the compressive strength of foamed concrete, the four machine learning regression models considered (*i.e.*, ELM, MARS, M5 Tree and SVR) were developed using MATLAB sub-routines. The construction of the models drew on an input matrix (x) defined by x = (cement content, oven-dry density, water binder ratio and foam volume data) represented as the predictor variables, while the target variable (y) was set as the compressive strength. In this process, 95% of the original total set of experimental input data were randomly selected and classified into the training set, and the remainder of data, unknown to the models, were classified into the validation and testing set. In order to investigate the relationship between compressive strength and each input data, and reaffirm the preciseness of the heuristic models, a study of significantly correlated concrete strength values with the respective predictors was undertaken.

Cross-correlation was performed by evaluating the value of r_{cross} ($-1.0 \le r_{\mathrm{cross}} \le +1.0$), determined between predictand ($y \equiv$ compressive strength) and the respective predictor (x), where r_{cross} was computed by a covariance function (Φ) for any x-value (lagged scale), where it was measured similarity between y and time-shifted $x_i = (x_1, x_2, \cdots, x_{P-1})$ with $y = (y_1, y_2, \cdots, y_{Q-1})$:

$$\begin{aligned} \Phi_{xy,\,k} &= \sum_{\min(P-1+k,\ Q-1)}^{j=\max(0,\ k)} y_{j-k}\ x_j \quad \text{where } k \\ &= -(P+1), \cdots, 0, \cdots, (Q-1) \end{aligned} \tag{27}$$

$$r_{cross}(lag = t) = \frac{\phi_{xy}(lag = t)}{\sqrt{\phi_{xx}(lag = 0)\cdot\phi_{yy}(lag = 0)}} \tag{28}$$

$$\Phi_{x_s x_s}(0) = \int_{-\infty}^{\infty} x(\tau)^2 d\tau \text{ and } \Phi_{y-y}(0) = \int_{-\infty}^{\infty} y(\tau)^2 d\tau \tag{29}$$

where: P, Q is the lag in x, y values; τ is the integral timescale; $\varphi_{xx}(0)$ is the autocorrelation function of x; $\varphi_{yy}(0)$ is the autocorrelation function of y, and $\varphi_{x-y}(t)$ is the cross-correlation function between x and y.

Fig. 4 displays the correlation of statistical indicators between each input candidate (x) including the data of cement content, oven dry density, water-to-binder ratio and foam content with respect to the target (y = compressive strength). The results reveal a statistically significant correlation with 95% confidence, indicating that the predictor and target variables selected for development of the heuristic models exhibit a significant relationship and are potentially suitable for generating the forecasted compressive strength values.

To construct the ELM model, a three-layer network with the neuronal architecture represented in Fig. 1 was employed. After data normalization, the most widely accepted transfer function comprised of the sigmoid equation was applied for feature extraction, in agreement with earlier studies [32,80]. To identify an optimal model architecture, a limit was set on the range of hidden neuron nodes (50–150) and each architecture was evaluated on a validation dataset to identify the optimal ELM architecture. Since an ELM model requires random initialization of its hidden layer parameters, the ELM model was run 500 times and computed the mean square error (*MSE*) for each hidden node. The network architecture that provided the smallest mean square error (*MSE*) in the independent (validation) set was selected as an optimal model.

To develop the MARS-based model, an ARESLab toolbox (version 1.13.0) [81] was adopted. The MARS model generally has two basis functions, which are made of cubic and linear piecewise equations. In

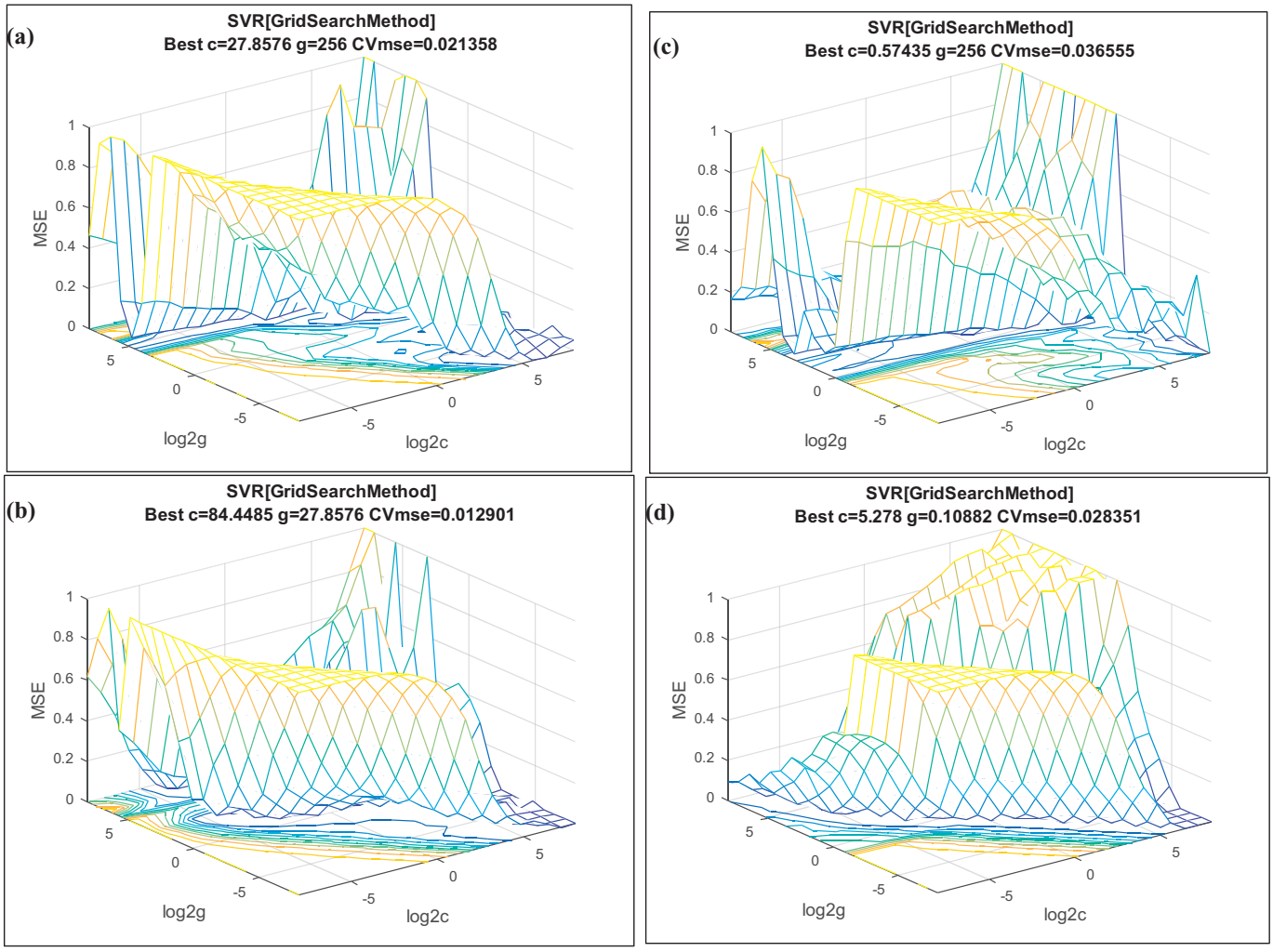

Fig. 4. The grid search algorithm parameters values in accordance to the mean square error (MSE) value with the following input variable: a) cement content, b) oven dry density, c) water binder, and d) foam content volume.

Table 1
Statistical performance indicators used to evaluate the model prediction accuracy. (*R* = correlation coefficient between observed and predicted data; *RMSE* = root mean square error; *MABE* = mean absolute bias error; *RRMSE* = relative *RMSE; MAPE* = relative *MABE*).

ELM								
Inputs	R	Willmott Index	Efficiency	Legates & McCabes Index	RMSE	MABE	RRMSE, %	MAPE, %
Cement content	0.875	0.885	0.610	0.400	3.247	2.629	39.502	60.775
Oven dry density	0.995	0.994	0.983	0.874	1.058	0.917	7.904	9.543
Water/binder ratio	0.941	0.924	0.785	0.607	3.803	2.741	28.469	52.844
Foam volume	0.983	0.986	0.964	0.829	1.482	1.194	15.030	20.689
MARS								
Cement content	0.885	0.888	0.499	0.245	3.681	3.312	44.786	43.746
Oven dry density	0.992	0.987	0.971	0.873	1.365	0.924	10.203	8.096
Water/binder ratio	0.935	0.789	0.388	0.274	6.409	5.060	47.973	97.304
Foam volume	0.956	0.933	0.794	0.542	3.566	3.202	36.168	66.513
M5 Model Tree								
Cement content	0.892	0.870	0.596	0.379	3.304	2.725	40.191	64.724
Oven dry density	0.970	0.973	0.928	0.744	2.168	1.868	16.202	18.580
Water/binder ratio	0.727	0.638	0.303	0.146	6.842	5.952	51.216	103.206
Foam volume	0.982	0.967	0.915	0.714	2.293	1.998	23.251	43.075
SVM								
Cement content	0.877	0.858	0.300	0.148	4.349	3.735	52.910	44.706
Oven dry density	0.965	0.928	0.804	0.564	3.571	3.180	26.686	29.203
Water/binder ratio	0.879	0.853	0.761	0.469	4.004	3.703	29.973	56.034
Foam volume	0.946	0.895	0.820	0.629	3.329	2.592	33.758	34.636

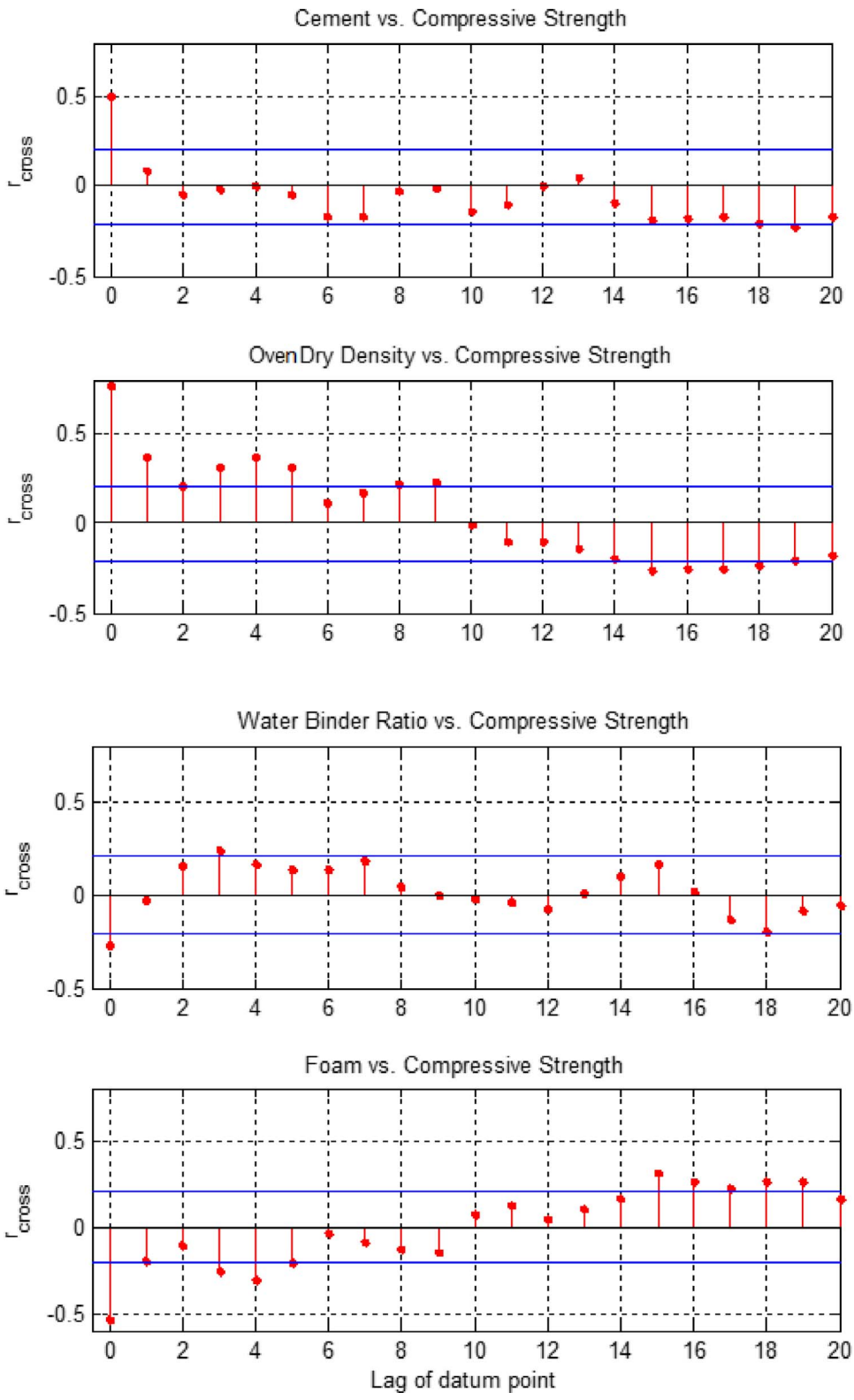

Fig. 5. Correlation statistical indicators between each input candidates including cement content, oven dry density, water-to-binder ratio and foam content versus compressive strength.

the present study, the cubic piecewise equation was adopted considering its greater smoothness and potentially better ability to extract pertinent features [82]. The generalized recursive partitioning regression (RPR) was employed for optimum function approximation [83] and the model development included dual phase (*i.e.*, forward and backward deletion process). In the forward phase, the MARS algorithm was executed with an initially 'naïve' model consisting of the intercept term, thereafter iteratively adding the reflected pair(s) of basis functions to yield the greatest decrease in training error (*RMSE*). The forward phase of the modelling continued until one of the following criteria was satisfied [80]: (i) the maximum number of basis functions reaches min [200, max(20, 2*d*) + 1], where d = the number of inputs [84], (ii) adding a new basis function changes the r^2 by less than a threshold value of 1×10^{-4}, (iii) r^2 reaches approximately 1.0, (iv) the number of basis functions (including the intercept term) is the same as the number of data observations, or (*v*) the number of effective

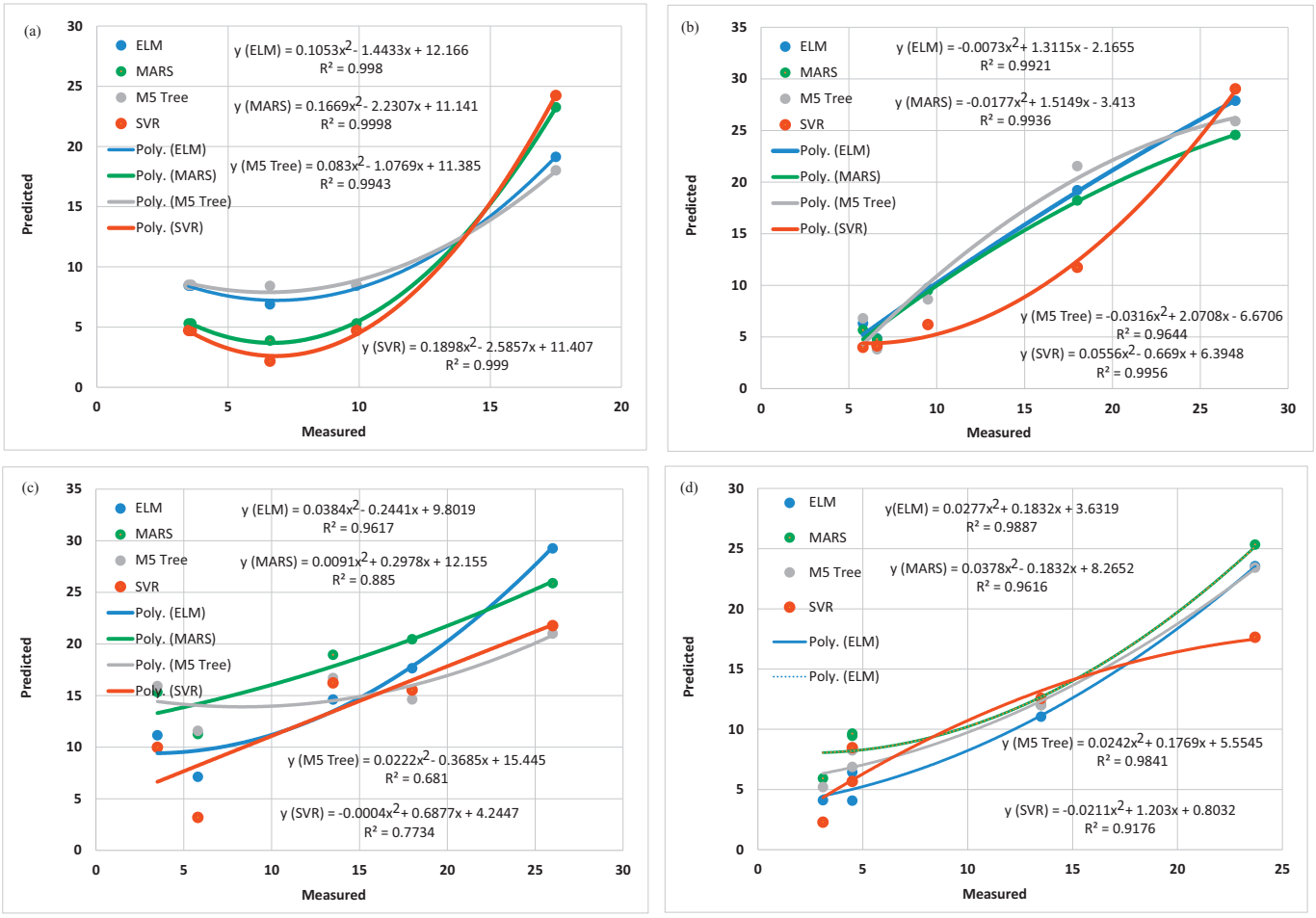

Fig. 6. Coefficient of determination (R^2) and polynomial equations for the four predictive models including ELM, MARS, M5 Tree and SVR. a) cement content, b) oven dry density, c) water binder ratio and d) foam content volume.

parameters reaches the number of data points. A large model generated at the end of the forward phase can potentially over-fit the data; therefore, the model was pruned by a backward pass by deleting redundant basis functions (*i.e.*, reducing the training error) until the model included only the intercept term. The model with lowest Generalized Cross-Validation (*GCV*) was selected.

The M5 Tree model was developed using the set of training parameters for model initialization where a minimum tree split value of 2.0, a smoothing value of 15 and a split threshold of 0.05 were selected in accordance to earlier work [46,80,85]. The model tree was pruned back implementing the 'divide-and-conquer rule' [44,60]. As such, the optimum number of decision-trees (or `rules') was determined via the model that attained the smallest value of the root mean square error and the largest correlation coefficient. This concurred with the standard deviation of class values and highest reduction in training error, resulting in a model with the best set of rules.

The SVR model was designed by employing a grid search procedure [32,46,71,86,87] used to determine the optimum regularisation constant and the RBF kernel width. To illustrate the primary model parameters, the chnages of the mean square error (MSE) in respect to the range of values of regularisation constants and kernel widths using the cement content, oven-dry density value, water binder and foam content values are plotted in Fig. 4. To concur with published literature [86–88], in this study it was evident that for a set combination of C and σ, the MSE attained was unique, revealing the different roles played by each input variable used for the prediction of concrete strength data. For all input combinations considered, the magnitude of these parameters were optimised to generate the most apppriate model.

5. Model performance indicators

In this paper, an analysis of the observed versus predicted compressive strength of lightweight foamed concrete (S) was conducted in conjunction with statistical metrics to appraise the accuracy of the ELM, MARS, M5 Tree and SVR model [89,90]. As a primary criterion, the root mean square error (*RMSE*), mean absolute error (*MAE*), their normalized equivalents expressed as a percentage, and the correlation coefficient (r) between observed (S^{obs}) and predicted (S^{pred}) data [89] were used as expressed below:

$$r = \frac{\sum_{i=1}^{i=N}[(S_i^{obs} - \overline{S^{obs}})\cdot(S_i^{pred} - \overline{S^{pred}})]}{\sqrt{\sum_{i=1}^{i=N}(S_i^{obs} - \overline{S^{obs}})^2 \cdot \sqrt{\sum_{i=1}^{i=N}(S_i^{pred} - \overline{S^{pred}})}}} \text{ where,}$$
$$-1 \le r \le 1 \quad (30)$$

$$RMSE = \sqrt{\frac{1}{N}\sum_{i=1}^{i=N}(S_i^{obs} - S_i^{pred})^2} \quad (31)$$

$$MAE = \frac{1}{N}\sum_{i=1}^{i=N}|S_i^{obs} - S_i^{pred}| \quad (32)$$

$$RRMSE = 100\cdot\frac{RMSE}{\overline{S^{obs}}} \quad (33)$$

$$RMAE = 100\cdot\frac{MAE}{\overline{S^{obs}}} \quad (34)$$

where: N is the number of datum points in the test period; S_i^{obs} is the i^{th}

observed S value; $\overline{S^{obs}}$ is the mean observed S value; S_i^{pred} is the i^{th} forecasted S value; and $\overline{S^{pred}}$ is the mean observed S value.

It should be noted that *RMSE* and *MAE* (presented in absolute units of S) are widely adopted to check the models' prediction accuracy via goodness-of-fit, (in absolute units) regardless of the sign of the difference between the predicted and observed data. While *MAE* provides an overall assessment of errors in the test set, *RMSE* is more appropriate when this error distribution is Gaussian [91]. Since the latter condition is not necessarily satisfied by all models, the *MAE*, which is not weighted towards higher or lower magnitudes and evaluates all deviations of predicted data from the observed values in an equal manner regardless of sign [76], should be employed. In addition, the *RRMSE* was utilized to examine the models' precision by comparing percentage deviation from predicted data, whereas the *RMAE* represents the average percentage magnitude of total absolute bias errors between predicted and observed data [92]. The commonly used coefficient of determination, r, was also employed to describe the covariance in observed data that can be explained by the prediction model.

Since the preceding statistics Eq. (30)–(34) are largely based on linear agreement between $S^{obs}$and S^{pred}, they can be overly sensitive to extreme values (outliers) in the observed data and somewhat insensitive to the additive or proportional differences between predictions and observations [93,94]. To address this limitation of *RMSE* and *MAE*, the Willmott's Index ($0 \le WI \le 1.0$) [94] and Nash-Sutcliffe coefficient ($-\infty \le E_{NS} \le 1.0$) were also calculated [95]:

$$E_{NS} = 1 - \left[\frac{\sum_{i=1}^{i=N} (S_i^{obs} - S_i^{pred})^2}{\sum_{i=1}^{i=N} (S_i^{obs} - \overline{S^{pred}})^2} \right] \quad (35)$$

$$WI = 1 - \left[\frac{\sum_{i=1}^{i=N} (S_i^{obs} - S_i^{pred})^2}{\sum_{i=1}^{i=N} (|S_i^{pred} - \overline{S^{obs}}| + |S_i^{obs} - \overline{S^{obs}}|)^2} \right] \quad (36)$$

Nash and Sutcliffe [95] introduced the E_{NS} as a measure to assess the deviation of the predicted/observed data from the overall means; consequently, assessing the agreement between observed and predicted S. However, E_{NS} uses the differences in observed and predicted means and variances of data [93,96]. In particular, the E_{NS} may overestimate larger values of observed data [93]. An improved measure of model accuracy with respect to *RMSE*, r and E_{NS}, is the *WI*, where the ratio of the mean square error and potential error is multiplied by the number of observations and then subtracted from one (1.0) to assess the squared differences. *WI* can overcome the issues associated with E_{NS} [94] since the ratio of the *RMSE* is considered rather than the square of the error difference [97]. As a cross-validation metric, the Legates and McCabe Index ($0 \le E_{LM} \le 1.0$) was also employed herein since this can present an advantage over *WI* when relatively high predicted values are expected, even for a poorly fitted model [97]. The E_{LM} [93] was utilized as a modified version of *WI* where the errors and differences are given appropriate weights without inflating their square values.

$$E_{LM} = 1 - \left[\frac{\sum_{i=1}^{i=N} |S_i^{obs} - S_i^{pred}|}{\sum_{i=1}^{i=N} |S_i^{obs} - \overline{S^{obs}}|} \right] \quad (37)$$

6. Application and evaluation of ELM and other machine learning regression models

Concrete is a heterogeneous composite of numerous constituents possibly including cement, water, fine and course aggregates, supplementary cementitious materials, chemical admixtures, and fibers. A major concern in concrete design is achieving and maintaining the specified compressive strength. Yet, this key property is highly dynamic, nonlinear and stochastic not only in terms of the mixture proportions, but also the consolidation and curing. The lack of the knowledgebase regarding the empirical relationship between concrete strength and its constituents has motivated researchers to explore novel and reliable soft computing and machine learning techniques that can mimic and capture those relationships. In the present study, four different machine learning models are examined to predict the compressive strength of lightweight foamed concrete. Different models are inspected based on input variables representing the cement content (Model 1), oven dry density (Model 2), water binder ratio (Model 3) and foamed volume (Model 4).

The statistical performance of the prediction of the investigated models is provided in Table 1. In terms of the cement content as the input variable (i.e., for Model 1), the ELM model showed the cement as an informative input candidate for the prediction process since the Nash Coefficient and Legates & McCabe's Index for this particular model far exceeded those of the other three machine learning models (*i.e.*, Nash = 0.610 vs. 0.499, 0.596 & 0.300; Legates & McCabe's Index = 0.400 vs. 0.245,0.379 & 0.148). This also concurred with the RMSE and MAE values revealing the better prediction capability of the ELM model compared to the counterpart models, and agrees well with Fig. 5 that illustrates that the cement content had a strong correlation with compressive strength. For the oven dry density as the input variable, the four predictive models exhibited different levels of accuracy. That is, Model 2 (which in fact, aimed to determine the sensitivity of the oven dry density for the prediction of compressive strength value) revealed that the ELM model had the highest correlation coefficient (i.e., R = 0.995) vs. 0.992, 0.970 & 0.965 for the MARS, M5 Tree and SVR model, respectively, between the measured and predicted compressive strength data.

Concurring very well with the relative predicted errors and the normalized prediction score metrics (Willmott's Index, Nash Efficiency and Legates and McCabe's Index), this result indicates that the over dry density (as a model's primary input) is also a very sensitive parameter that acts to determine the overall compressive strength. Fig. 6 shows

Table 2
Relative error (%) for each test data points between predicted and measured concrete strength in test period for the ELM, MARS, M5 Tree and SVR models.

Input combination and model	Relative error - ELM model, %	Relative error - MARS model, %	Relative error - M5 Tree model, %	Relative error SVM model, %
M1: (input = cement)				
	−134.503	−46.9307	−136.23	−30.8518
	−4.14569	41.25482	−27.3984	67.22264
	−141.203	−51.1287	−142.98	−34.5905
	14.72607	46.57067	14.09809	52.41752
	−9.29607	−32.844	−2.9144	−38.4459
Mean Relative Error	−54.8845	−8.6156	−59.0849	3.150
M2: (input = Oven dry Density)				
	−2.48777	−0.00888	9.160987	34.78673
	−8.89021	2.524339	−17.3171	31.23722
	−3.27009	8.990184	4.092983	−7.5359
	−6.74462	−1.19268	−19.7225	34.79382
	26.32003	27.76548	42.6076	37.6625
Mean Relative Error*	0.9855	7.6157	3.7644	26.1889
M3: (input = water/ binder)				
	−22.7853	−94.1823	−99.7272	45.0675
	−12.5435	0.456962	19.20739	16.28837
	−8.26374	−40.3187	−23.6547	−20.1738
	−218.678	−337.955	−354.699	−184.914
	1.948441	−13.6068	18.74179	13.72506
Mean Relative Error	−52.0644	−97.1211	−88.0264	−26.001
M4: (input = foam)				
	9.619402	−109.977	−52.6946	−25.9478
	−32.2194	−90.6615	−67.3267	26.64585
	0.645612	−6.86997	1.210746	25.58711
	−42.6939	−114.017	−82.9486	−88.0281
	18.26722	11.03751	11.19593	6.9731
Mean Relative Error	−9.27621	−62.0976	−38.1126	−10.9540

Table 3
Average values of coefficient of determination for the four predictive models including ELM, MARS, M5 Tree and SVR.

Models	M1 cement content	M2 oven dry density	M3 water/ binder	M4 foam content	Average correlation
ELM	99.80	99.21	96.17	98.87	98.51
MARS	99.98	99.36	88.50	96.16	96.00
M5-Tree	99.43	96.44	68.10	98.41	90.60
SVM	99.90	99.56	77.34	91.76	92.14

the trend of the correlation between experimental and predicted compressive strength for the four models with the variable cement content.

For the oven dry density, the four different modelling techniques were used to predict the compressive strength for specimens having different densities, and therefore, exhibited different degrees of accuracy. The second order polynomial representation and coefficient of determination were identically for the ELM model (Fig. 6b).

The four predictive models were also used to inspect the effect of the fundamental parameter water binder ratio (w/b) on the compressive strength of the foamed concrete. Model 3 revealed best correlation coefficient attained between measured and predicted compressive strength with R = 0.941, 0.935, 0.727 and 0.879 for ELM, MARS, M5 Tree and SVR models, respectively. The second order polynomial representation was close to the measured data using the ELM model than that of the other predictive models. Fig. 6c exhibits the trend of actual versus predicted compressive strength for the three versus variable w/b ratio.

The foam content was the fourth variable explored by the four modelling techniques to investigate its effective on the overall compressive strength. The values indicating the best goodness-fit (i.e. correlation coefficient) were 0.983, 0.956, 0.982 and 0.946, respectively for the ELM, MARS, M5 Tree and SVR models. The regression graph representing the second order polynomial achieved the best fit between measured and predicted strength data simulated by the ELM model (Fig. 6d).

Further model evaluation was conducted via the relative error percentage (RE) for each tested datum point which can be best expressed as:

$$RE = \frac{S_i^{obs} - S_i^{pred}}{S_i^{obs}} * 100 \tag{38}$$

The RE values for the four predictive models and for the four input

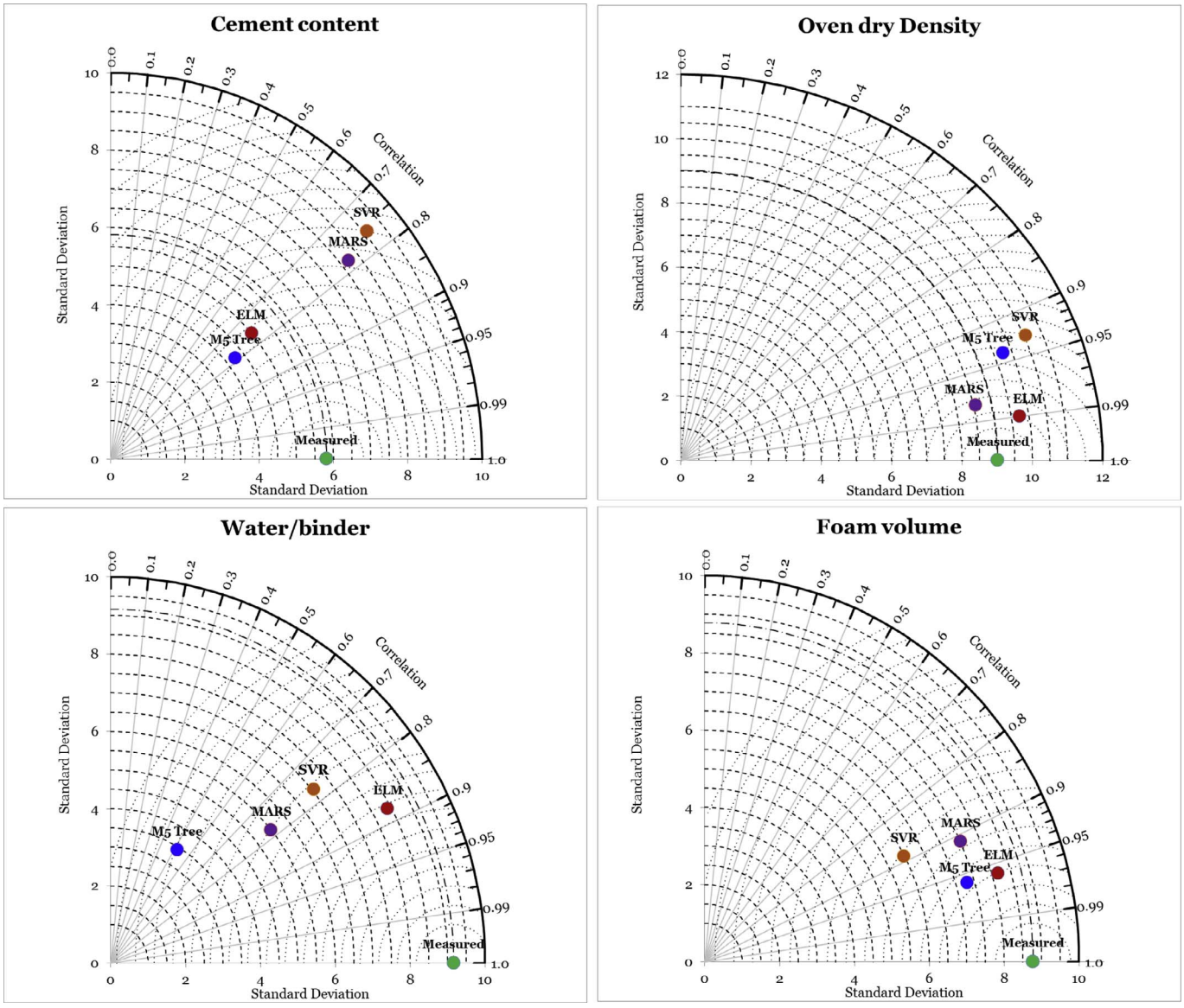

Fig. 7. Taylor diagram graphical presentation for the four predictive models including ELM, MARS, M5 Tree and SVR. The optimal prediction skill is observed for the ELM model.

combinations are tabulated in Table 2. It can be deduced that this evaluator expresses more details for under- and over-estimation of the compressive concrete strength. Generally, the ELM model yielded the most acceptable level of prediction using the oven dry density as an input variable with mean value equal to 0.98%.

A summary of the coefficients of determination for the four constitutive parameters and the four predictive models considered in the present study is presented Table 3. It can be observed that the various models achieved the best predictive capability for the effects of the four input variables explored. However, the ELM modelling technique achieved the highest overall average coefficient of determination (R^2 = 0.9851) among the four modelling approaches. It can thus be argued that the ELM model constitutes a reliable, accurate and intelligent approach for predicting the compressive strength of foamed concrete and should be explored as a predictive tool for other engineering properties of various types of concrete in general. This intelligent, rapid and cost-effective approach for predicting compressive strength can allow reducing the extent of trial batches, thus accelerating construction schedules. It could also provide a tool to confirm laboratory data that could involve human and equipment errors. For instance, in the case of predicting the 28 days' concrete strength in accordance to the project standards.

For a more comprehended presentation, the predictive models (ELM and the comparative models) are examined using graphical demonstration of Taylor diagram [98], as displayed in Fig. 7. In this way, all of the applied data-driven models can be visualized in terms of how closely they are in terms of predicting the actual target variable (i.e., compressive strength). Two different statistical metrics (i.e., correlation coefficients and standard deviations of each model) are used for quantifying the comparability between the prescient models and the corresponding measured records. The distance from the reference point (i.e., measured) is a measure of the centered RMSE. A perfect predictive model (being in full concurrence with the observations) is set apart by the reference point with the correlation coefficient equivalent to 1, and a similar abundancy of varieties contrasted with the observations. Based on the graphs presentation of the four input variables, ELM model performed quite well (i.e., being most accurate) in comparison to the MARS, M5 Tree and the SVR model. This is particularly enshrined for the case of the oven dry density as a predictor for the compressive concrete strength as the target. It is therefore admissible that the ELM model outperforms all other machine learning models applied in this context of estimating the compressive strength data.

7. Summary and conclusions

The present research is an early study for using the regression-based soft computing model called Extreme Learning Machine, ELM (i.e., an improved version of neural network models) for predicting the compressive strength of lightweight foamed concrete. The model prediction of the ELM has been validated comparatively with three robust regression data-driven models including the MARS, M5 Tree and SVR. The main constitutive input parameters used to establish the modeling techniques included the cement content, oven dry density, water binder ratio and foamed volume. An experimental database was created using relevant experimental data retrieved from the open literature, as displayed in the appendix section. Various statistical performance indicators were used to explore the predictive capability of the four modeling techniques. It can be concluded that the four models achieved superior predictive capability for the effects of various influential input variables on the compressive strength. However, the ELM modelling technique achieved best overall predictive performance among the four modelling approaches. The ELM model offers therefore a reliable, accurate and intelligent approach for predicting the compressive strength of foamed concrete and should be explored as a predictive tool for other engineering properties of cementitious materials. Such a model can be part of the portfolio of tools used by construction engineers in decision making, with minimum trial batches and less time-consuming laboratory and field testing validation. This tool is flexible and highly adaptable since it could be easily extended to cover a wider scope of experimental data and different engineering properties pertaining to the rheology, mechanical properties, durability and sustainability of civil infrastructure.

Acknowledgement

Experimental data used in modeling development in the present study were retrieved from the open literature. All data sources are acknowledged.

Appendix 1. The experimental data set utilized in the current research to predict compressive light concrete strength [2,4,6,8–10]

Cement	Over dry density	Water binder ratio	Foam volume	Compressive strength	Cement	Over dry density	Water binder ratio	Foam volume	Compressive strength
1154	1410	0.3	208	23	500	1466	0.5	295	15
1167	1400	0.29	188	18	500	1470	0.5	295	17.5
1160	1400	0.29	173	11	670	1450	0.5	295	20.5
385	950	0.3	470	5.2	500	1480	0.325	295	25.5
259	950	0.29	460	4	500	1476	0.325	295	27
193	950	0.29	450	2.1	686	1475	0.325	295	33.5
400	1490	0.7	260	9.9	500	1778	0.525	166	23
400	1100	0.7	430	5.2	744	1797	0.35	166	47
400	660	0.7	590	2.3	500	1457	0.5	233	22.5
686.1	1520	0.31	300	23.7	686	1468	0.325	233	36.5
970.8	1160	0.3	370	17	1204	1860	0.5	0	49.4
431	960	0.310	540	4.2	962	1400	0.5	208	23.4
581.9	710	0.300	630	6.6	722	920	0.5	404	11.8
887	1220	0.24	510	34.2	602	880	0.5	507	7.7
1317	1550	0.22	270	44.1	482	660	0.5	673	2.8
411	631	0.44	770	2.07	1468	2020	0.35	0	77.3
179.5	678	0.42	716	0.71	1174	1500	0.35	228	35.2
311	497	0.45	886	1.09	877	1150	0.35	432	11.3
325	1396	0.5	400	0.25	734	940	0.35	524	4.5
844	1338	0.57	164	0.23	588	740	0.35	623	2.7
825	1304	0.57	204	1.1	750	924	0.4	300	5.8

(continued on next page)

(continued)

Cement	Over dry density	Water binder ratio	Foam volume	Compressive strength	Cement	Over dry density	Water binder ratio	Foam volume	Compressive strength
500	1310	0.3	415.1	21	634	782	0.4	380	4.4
500	1505	0.3	341.5	27	514	562	0.4	360	2.4
500	1710	0.3	267.8	43	386	388	0.4	270	0.6
500	1300	0.3	408.2	9	38	650	0.5	630	18.5
500	1510	0.3	332.7	21	57	1000	0.5	450	5.5
500	1705	0.3	257.3	26	848	1155	0.33	380	9.22
500	1300	0.26	418.9	21	600	910	0.32	450	5.8
500	1305	0.26	418.9	25	600	880	0.32	520	3.9
500	1310	0.26	418.9	32	600	895	0.32	500	3.6
500	1505	0.26	342.8	26	600	925	0.33	430	3.5
500	1510	0.26	342.8	33	600	1105	0.32	410	6.8
500	1515	0.26	342.8	38	600	1120	0.32	400	4.7
400	595	0.35	700	3.1	600	1090	0.33	410	4.5
400	700	0.35	650	4.7	600	1130	0.33	400	4.3
400	640	0.35	600	3.6	460	1520	0.31	300	23.7
400	690	0.35	600	4.5	650	1160	0.3	370	17
400	675	0.4	650	3.6	290	960	0.31	540	4.2
400	620	0.4	700	3.5	390	710	0.3	630	6.6
400	635	0.4	0	4.3	185	1200	0.4	450	4.8
500	1137	0.475	420	6	400	1450	0.8	350	10.5
500	1139	0.475	420	6.5	600	950	0.6	430	7.2
612	1125	0.475	420	9.5	400	860	0.9	690	9.3
500	1155	0.3	420	13	461	1220	0.24	510	34.2
500	1159	0.3	420	13.5	550	1450	0.42	470	38.3
628	1147	0.3	420	19					

References

[1] Nambiar EK, Ramamurthy K. Air void characterisation of foam concrete. Cem Concr Res 2007;37:221–30.
[2] Jones M, McCarthy A. Preliminary views on the potential of foamed concrete as a structural material. Mag Concr Res 2005;57:21–31.
[3] Ramamurthy K, Kunhanandan Nambiar EK, Indu Siva Ranjani G. A classification of studies on properties of foam concrete. Cem Concr Compos 2009;31:388–96.
[4] Kearsley E, Wainwright P. The effect of high fly ash content on the compressive strength of foamed concrete. Cem Concr Res 2001;31:105–12.
[5] Hilal AA, Thom NH, Dawson AR. On void structure and strength of foamed concrete made without/with additives. Construct Build Mater 2015;85:157–64.
[6] Pan Z, Hiromi F, Wee T. Preparation of high performance foamed concrete from cement, sand and mineral admixtures. J Wuhan Univ Technol 2007;22:295–8.
[7] Jones MR, McCarthy A. Heat of hydration in foamed concrete: effect of mix constituents and plastic density. Cem Concr Res 2006;36:1032–41.
[8] Sun HY, Gong AM, Peng YL, Wang X. The study of foamed concrete with polypropylene fiber and high volume fly ash. Appl Mech Mater 2011;90:1039–43.
[9] Hilal AA, Thom NH, Dawson AR. The use of additives to enhance properties of preformed foamed concrete. Int J Eng Technol 2015;7:286–93.
[10] Tikalsky PJ, Pospisil J, MacDonald W. A method for assessment of the freeze–thaw resistance of preformed foam cellular concrete. Cem Concr Res 2004;34:889–93.
[11] Yen LB. Study of water ingress into foamed concrete. National University of Singapore; 2007.
[12] Mydin MAO, Wang YC. Mechanical properties of foamed concrete exposed to high temperatures. Construct Build Mater 2012;26:638–54.
[13] Hilal AA, Thom NH, Dawson AR. Pore structure and permeation characteristics of foamed concrete. J Adv Concr Technol 2014;12:535–44.
[14] Narayanan N, Ramamurthy K. Microstructural investigations on aerated concrete. Cem Concr Res 2000;30:457–64.
[15] Nambiar EKK, Ramamurthy K. Air void characterisation of foam concrete. Cem Concr Res 2007;37:221–30.
[16] Hilal AA, Thom NH, Dawson AR. On entrained pore size distribution of foamed concrete. Construct Build Mater 2015;75:227–33.
[17] Kozłowski M, Kadela M, Kukiełka A. Fracture energy of foamed concrete based on three-point bending test on notched beams. Proc Eng 2015;108:349–54.
[18] Hilal AA, Thom NH, Dawson AR. Failure mechanism of foamed concrete made with/without additives and lightweight aggregate. J Adv Concr Technol 2016;14:511–20.
[19] Sayadi AA, Vilches TJ, Neitzert TR, Clifton GC. Strength of bearing area and locking area of galvanized strips in foamed concrete. Construct Build Mater 2016;114:56–65.
[20] Narayanan N, Ramamurthy K. Structure and properties of aerated concrete: a review. Cem Concr Compos 2000;22:321–9.
[21] Nehdi M, Djebbar Y, Khan A. Neural network model for preformed-foam cellular concrete. ACI Mater J 2001;98:402–9.
[22] Kearsley E, Wainwright P. The effect of porosity on the strength of foamed concrete. Cem Concr Res 2002;32:233–9.
[23] Khan MI. Predicting properties of High Performance Concrete containing composite cementitious materials using Artificial Neural Networks. Autom Construct 2012;22:516–24.
[24] Casasent D, Chen XW. Radial basis function neural networks for nonlinear Fisher discrimination and Neyman–Pearson classification. Neural Netw 2003;16:529–35.
[25] Altun F, Ö K, Aydin K. Predicting the compressive strength of steel fiber added lightweight concrete using neural network. Comput Mater Sci 2008;42:259–65.
[26] Bilim C, Atiş CD, Tanyildizi H, Karahan O. Predicting the compressive strength of ground granulated blast furnace slag concrete using artificial neural network. Adv Eng Softw 2009;40:334–40.
[27] Atici U. Prediction of the strength of mineral admixture concrete using multivariable regression analysis and an artificial neural network. Expert Syst Appl 2011;38:9609–18.
[28] Alshihri MM, Azmy AM, El-Bisy MS. Neural networks for predicting compressive strength of structural light weight concrete. Construct Build Mater 2009;23:2214–9.
[29] Demir F. Prediction of elastic modulus of normal and high strength concrete by artificial neural networks. Construct Build Mater 2008;22:1428–35.
[30] Huang G-B, Chen L. Convex incremental extreme learning machine. Neurocomputing 2007;70:3056–62.
[31] Huang GB, Chen L, Siew CK. Universal approximation using incremental constructive feedforward networks with random hidden nodes. IEEE Trans Neural Netw 2006;17:879–92.
[32] Deo RC, Tiwari MK, Adamowski JF, Quilty MJ. Forecasting effective drought index using a wavelet extreme learning machine (W-ELM) model. Stoch Environ Res Risk A 2016:1–30.
[33] Deo RC, Şahin M. An extreme learning machine model for the simulation of monthly mean streamflow water level in eastern Queensland. Environ Monit Assess 2016. http://dx.doi.org/10.1007/s10661-016-5094-9.
[34] Deo RC, Şahin M. Application of the extreme learning machine algorithm for the prediction of monthly effective drought index in eastern Australia. Atmos Res 2015;153:512–25.
[35] Yaseen ZM, Jaafar O, Deo RC, Kisi O, Adamowski J, Quilty J, et al. Stream-flow forecasting using extreme learning machines: a case study in a semi-arid region in Iraq. J Hydrol 2016.
[36] Huang G-B, Zhu Q-Y, Siew C-K. Extreme learning machine: theory and applications. Neurocomputing 2006;70:489–501.
[37] Huang G-B, Zhou H, Ding X, Zhang R. Extreme learning machine for regression and multiclass classification. IEEE Transa Syst Man Cybern Part B 2012;42:513–29.
[38] Huang G, Huang G-B, Song S, You K. Trends in extreme learning machines: a review. Neural Netw 2015;61:32–48.
[39] Acharya N, Shrivastava N, Panigrahi B, Mohanty U. Development of an artificial neural network based multi-model ensemble to estimate the northeast monsoon rainfall over south peninsular India: an application of extreme learning machine. Clim Dyn 2013;43:1303–10.
[40] Huang, G.-B., Zhu, Q.-Y., Siew, C.-K. Extreme learning machine: theory and applications. 2006. p. 489–501.
[41] Friedman JH. Multivariate adaptive regression splines. Ann Statist 1991:1–67.
[42] Sharda V, Prasher S, Patel R, Ojasvi P, Prakash C. Performance of Multivariate Adaptive Regression Splines (MARS) in predicting runoff in mid-Himalayan micro-watersheds with limited data/Performances de régressions par splines multiples et adaptives (MARS) pour la prévision d'écoulement au sein de micro-bassins versants Himalayens d'altitudes intermédiaires avec peu de données. Hydrol Sci J 2008;53:1165–75.
[43] Deo RC, Samui P, Kim D. Estimation of monthly evaporative loss using relevance vector machine, extreme learning machine and multivariate adaptive regression

spline models. Stoch Environ Res Risk A 2015:1–16.
[44] Kisi O. Pan evaporation modeling using least square support vector machine, multivariate adaptive regression splines and M5 model tree. J Hydrol 2015;528:312–20.
[45] Waseem M, Ajmal M, Kim T-W. Development of a new composite drought index for multivariate drought assessment. J Hydrol 2015;527:30–7.
[46] Deo RC, Kisi O, Singh VP. Drought forecasting in eastern Australia using multivariate adaptive regression spline, least square support vector machine and M5Tree model. Atmos Res 2017;184:149–75.
[47] Krzyscin J, Eerme K, Janouch M. Long-term variations of the UV-B radiation over Central Europe as derived from the reconstructed UV time series. Annales Geophysicae 2004:1473–85.
[48] Krzyścin J. Nonlinear (MARS) modeling of long-term variations of surface UV-B radiation as revealed from the analysis of Belsk, Poland data for the period 1976–2000. Annales Geophysicae 2003:1887–96.
[49] Krzyscin JW. Long-term changes in ozone mini-hole event frequency over the northern hemisphere derived from ground-based measurements. Int J Climatol 2002;22:1425–39.
[50] Aun M, Eerme K, Aun M, Ansko I. Reconstruction of UVB and UVA radiation at Tõravere, Estonia, for the years 1955-2003. Proc Estonian Acad Sci 2016;65:50.
[51] Krzyscin, J. Non-linear (mars) modeling of the long-term variations of surface uv-b radiation: as revealed from the analysis of Belsk, Poland, Uv Data For The Period 1976–2000. EGS General Assembly Conference Abstracts2002. p. 1219.
[52] Cheng M-Y, Cao M-T. Accurately predicting building energy performance using evolutionary multivariate adaptive regression splines. Appl Soft Comput 2014;22:178–88.
[53] Butte NF, Wong WW, Adolph AL, Puyau MR, Vohra FA, Zakeri IF. Validation of cross-sectional time series and multivariate adaptive regression splines models for the prediction of energy expenditure in children and adolescents using doubly labeled water. J Nutr 2010;140:1516–23.
[54] Sephton P. Forecasting recessions: can we do better on MARS. Fed Res Bank St Louis Rev 2001;83.
[55] Zhang W, Goh A. Multivariate adaptive regression splines for analysis of geotechnical engineering systems. Comput Geotech 2013;48:82–95.
[56] Craven P, Wahba G. Smoothing noisy data with spline functions. Numerische Mathematik 1978;31:377–403.
[57] Samui P. Slope stability analysis using multivariate adaptive regression spline. Metaheuristics in water, geotechnical and transport engineering 327. 2012.
[58] Quinlan JR. Learning with continuous classes. 5th Australian joint conference on artificial intelligence. 1992. p. 343–8.
[59] Mitchell TM. Machine learning. Machine learning. Burr Ridge: McGraw-Hill; 1997. MATH. 1997.
[60] Rahimikhoob A, Asadi M, Mashal M. A comparison between conventional and M5 model tree methods for converting pan evaporation to reference evapotranspiration for semi-arid region. Water Resour Manag 2013;27:4815–26.
[61] Bhattacharya B, Solomatine DP. Neural networks and M5 model trees in modelling water level–discharge relationship. Neurocomputing 2005;63:381–96.
[62] Witten, I.H., Frank, E.. Data mining: practical machine learning tools and techniques: Morgan Kaufmann; 2005.
[63] Smola AJ, Schölkopf B. A tutorial on support vector regression. Statist Comput 2004;14:199–222.
[64] Salcedo-Sanz S, Rojo-Álvarez J, Martínez-Ramón M, Camps-Valls G. Support vector machines in engineering: an overview. Wiley Interdisciplinary Rev 2014;4:234–67.
[65] Vapnik VN, Vapnik V. Statistical learning theory. New York: Wiley; 1998.
[66] Suykens JAK, Lukas L, Van Dooren P DMB, Vandewalle J. Least squares support vector machine classifiers: a large scale algorithm. European Conference on Circuit Theory and Design, ECCTD. Citeseer; 1999. p. 839–42.
[67] Suykens JAK, Vandewalle J. Least squares support vector machine classifiers. Neural Process Lett 1999;9:293–300.
[68] Bishop CM. Neural networks for pattern recognition. Oxford university press; 1995.
[69] Cherkassky V, Mulier FM. Learning from data: concepts, theory, and methods. John Wiley & Sons; 2007.
[70] Müller K-R, Smola AJ, Rätsch G, Schölkopf B, Kohlmorgen J, Vapnik V. Predicting time series with support vector machines. Artificial Neural Networks—ICANN'97. Switzerland: Springer Berlin Heidelberg; 1997. p. 999–1004.
[71] Deo RC, Samui P. Forecasting evaporative loss by least-square support-vector regression and evaluation with genetic programming, Gaussian process, and minimax probability machine regression: case study of Brisbane City. J Hydrol Eng 2017:05017003.
[72] Suykens JAK, De Brabanter J LL, Vandewalle J. Weighted least squares support vector machines: robustness and sparse approximation. Neurocomputing 2002;48:85–105.
[73] Okkan U, Serbes ZA. Rainfall–runoff modeling using least squares support vector machines. Environmetrics 2012;23:549–64.
[74] Goyal MK, Bharti B, Quilty J, Adamowski J, Pandey A. Modeling of daily pan evaporation in sub tropical climates using ANN, LS-SVR, Fuzzy Logic, and ANFIS. Expert Syst Appl 2014;41:5267–76.
[75] Deo RC, Wen X, Feng Q. A wavelet-coupled support vector machine model for forecasting global incident solar radiation using limited meteorological dataset. Appl Energy 2016;168:568–93.
[76] Deo RC, Tiwari MK, Adamowski J, Quilty J. Forecasting effective drought index using a wavelet extreme learning machine (W-ELM) model. Stoch Environ Res Risk A 2017. http://dx.doi.org/10.1007/s00477-016-1265-z. in press.
[77] Ortiz-García EG, Salcedo-Sanz S, ÁM P-B, Portilla-Figueras JA. Improving the training time of support vector regression algorithms through novel hyper-parameters search space reductions. Neurocomputing 2009;72:3683–91.
[78] Hiromi F, Wee T. Preparation of high performance foamed concrete from cement, sand and mineral admixtures. Journal of Wuhan Univ Technol Mater Sci Ed 2007;22:295–8.
[79] Sun HY, Gong AM, Peng YL, Wang X. The study of foamed concrete with polypropylene fiber and high volume fly ash. Appl Mech Mater 2011:1039–43.
[80] Deo RC, Downs N, Parisi A, Adamowski J, Quilty J. Very short-term reactive forecasting of the solar ultraviolet index using an extreme learning machine integrated with the solar zenith angle. Environ Res 2017;155:141–66.
[81] Jekabsons G. Adaptive regression splines toolbox for Matlab/Octave. version 1. 2013. p. 72.
[82] Kooperberg C, Clarkson DB. Hazard regression with interval-censored data. Biometrics 1997:1485–94.
[83] Zareipour H, Bhattacharya K, Canizares C. Forecasting the hourly Ontario energy price by multivariate adaptive regression splines. IEEE Power Engineering Society General Meeting. 2006. IEEE; 2006. 7 pp.
[84] Milborrow, S. Multivariate Adaptive Regression Splines. Package 'earth': Derived from mda:mars by Trevor Hastie and Rob Tibshirani Uses Alan Miller's Fortran utilities with Thomas Lumley's leaps wrapper. 2016; URL http://www.milbo.users.sonic.net/earth.
[85] Wang YW. IH: Inducing model trees for predicting continuous classes. Proceedings of European Conference on Machine Learning University of Economics Prague. 1997.
[86] Hsu C-W, Chang C-C, Lin C-J. A practical guide to support vector classification. 2003.
[87] Lin H-T, Lin C-J. A study on sigmoid kernels for svm and the training of non-psd kernels by smo-type methods. Technical report, Department of Computer Science, National Taiwan University, Taipei, Taiwan. 2003.
[88] Hsu H-H, Hung C-H, Lo A-K, Wu C-C, Hung C-W. Influence of tropical cyclones on the estimation of climate variability in the tropical western North Pacific. J Climatol 2008;21:2960–75.
[89] Krause P, Boyle D, Bäse F. Comparison of different efficiency criteria for hydrological model assessment. Adv Geosci 2005;5:89–97.
[90] Dawson CW, Abrahart RJ, See LM. HydroTest: a web-based toolbox of evaluation metrics for the standardised assessment of hydrological forecasts. Environ Model Softw 2007;22:1034–52.
[91] Chai T, Draxler RR. Root mean square error (RMSE) or mean absolute error (MAE)?–Arguments against avoiding RMSE in the literature. Geosci Model Dev 2014;7:1247–50.
[92] Mohammadi K, Shamshirband S, Tong CW, Arif M, Petković D, Ch S. A new hybrid support vector machine–wavelet transform approach for estimation of horizontal global solar radiation. Energy Convers Manag 2015;92:162–71.
[93] Legates DR, McCabe GJ. Evaluating the use of "goodness of fit" measures in hydrologic and hydroclimatic model validation. Water Resour Res 1999;35:233–41.
[94] Willmott CJ. On the validation of models. Phys Geogr 1981;2:184–94.
[95] Nash J, Sutcliffe J. River flow forecasting through conceptual models part I—A discussion of principles. J Hydrol 1970;10:282–90.
[96] NERC. Flood studies report vol. 1. London, UK: Hydrological Studies. Natural Environment Research Council; 1975.
[97] Willmott CJ. On the evaluation of model performance in physical geography. Spatial statistics and models. Springer; 1984. p. 443–60.
[98] Taylor KE. Summarizing multiple aspects of model performance in a single diagram. J Geophys Res Atmos 2001;106:7183–92. http://dx.doi.org/10.1029/2000JD900719.